INTERNATIONAL JOURNAL FOR NUMERICAL METHODS IN ENGINEERING, VOL. 21, 65–88 (1985)

A SOLUTION METHOD FOR PLANAR AND AXISYMMETRIC CONTACT PROBLEMS

KLAUS-JÜRGEN BATHE† AND ANIL CHAUDHARY‡

Massachusetts Institute of Technology, Cambridge, Massachusetts, U.S.A.

SUMMARY

A solution procedure for the analysis of planar and axisymmetric contact problems involving sticking, frictional sliding and separation under large deformations is presented. The contact conditions are imposed using the total potential of the contact forces with the geometric compatibility conditions, which leads to contact system matrices and force vectors. Some key aspects of the procedure are the contact matrices, the use of distributed tractions on the contact segments for deciding whether a node is sticking, sliding or releasing and the evaluation of the nodal point contact forces. The solutions to various sample problems are presented to demonstrate the applicability of the algorithm.

1 INTRODUCTION

Much progress has been made during recent years in the development of computational capabilities for general analysis of certain nonlinear effects in solids and structures. In each of these developments, quite naturally, the first step was the demonstration of some ideas and possibilities for the analyses under consideration, and then the research and development for reliable and general techniques was undertaken. The second step proved in many cases much more difficult, and in the case of capabilities for analysis of contact problems has yielded few general results.

Although some of the first complex contact problems have been solved using the finite element method quite some time ago,[1–3] and much interest exists in the research and solution of contact problems (see, for example, References 4–15), there is still a great deal of effort necessary for the development of a reliable, general and cost-effective algorithm for the *practical* analysis of such problems. This is largely due to the fact that the analysis of contact problems is computationally extremely difficult, even for the simplest constitutive relations used. Much of the difficulty lies in that the boundary conditions of the bodies under consideration are not known prior to the analysis, but they depend on the solution variables.

The aim in our research is the development of a solution algorithm for analysis of general contact conditions which shall include the possibilities to analyse: contact between flexible–flexible and rigid–flexible bodies; sticking or sliding conditions (with or without friction); large relative motions between bodies; repeated contact and separation between the bodies.

Since the large deformation motion of the individual bodies can in many cases be analysed already quite effectively,[16] an algorithm of the above nature will certainly enlarge, very

†Professor of Mechanical Engineering.
‡Research Assistant.

0029 5981/85/010065–24$02.40

Received May 1983
Revised November 1983

significantly, the currently available computational capabilities for practical nonlinear analyses. The objective in this paper is to present our first research results towards the above aim.

In this paper we consider the large deformation motion of two-dimensional planar or axisymmetric bodies in contact, and in static conditions. The algorithm we present contains the following major ingredients:

1. The total potential of the contact forces is included in the variational formulation to enforce the geometric compatibilities along the contact surfaces.
2. In the region of contact, surface tractions are evaluated from the externally applied forces, the nodal point forces equivalent (in the virtual work sense) to the current element stresses and Coulomb's law of friction.
3. The surface tractions between nodal points (on the element segments) are employed to decide whether a nodal point is in sticking or sliding contact, or is releasing.
4. The number of equations due to the contact conditions is dynamically adjusted to solve two equations for each node in contact if the node is in sticking condition, and one equation if the node is in sliding condition.

Because of the highly nonlinear contact conditions to be analysed, the success of the algorithm largely depends on an effective formulation with special attention to details.

In the next two sections we present the formulation of the algorithm and the important numerical aspects. We have implemented the solution method in the computer program ADINA,[17] and in Section 4 we give the solutions to various sample problems. These serve to demonstrate the applicability of and also the assumptions used in the algorithm.

2 FORMULATION OF CONTACT PROBLEM

Figure 1 shows schematically the problem we consider. This figure shows two generic bodies which we arbitrarily denote as *contactor* and *target*. In the finite element solution, the contactor contains the finite element boundary nodes that come into contact with the target segments or nodes. Although only two bodies are shown to come into contact, the algorithm can analyse the contact conditions between a number of bodies.

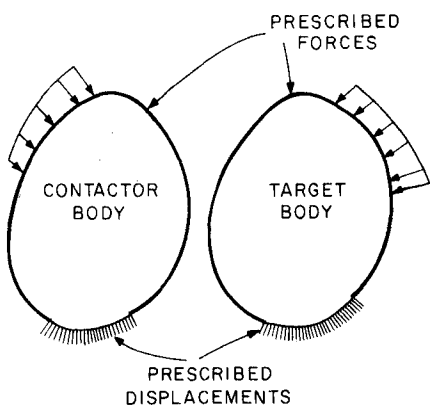

(a) Condition prior to contact

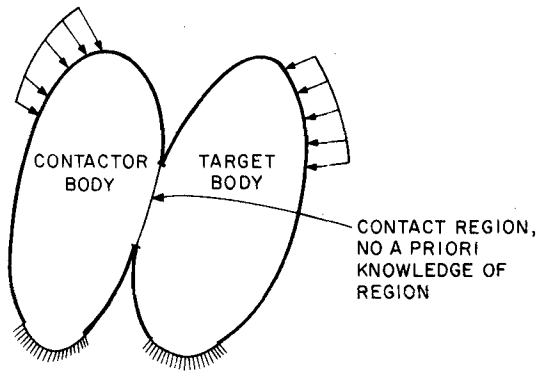

(b) Condition at contact

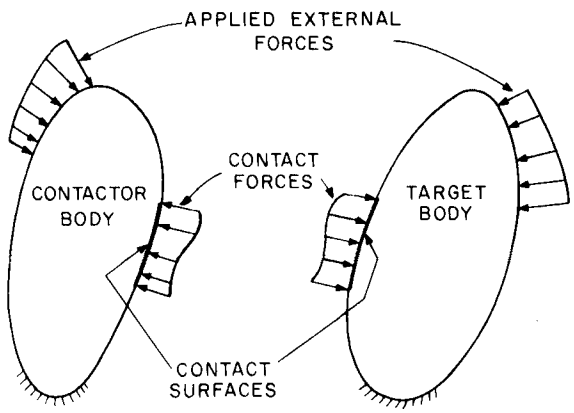

(c) Forces acting on contactor and target bodies

Figure 1. Schematic representation of problem considered

The basic conditions of contact along the contact surfaces are that no material overlap can occur, and as a result, contact forces are developed that act along the region of contact upon the target and the contactor. These forces are equal and opposite. The normal tractions can only exert compressive action, and the tangential tractions satisfy a law of frictional resistance.

The friction law used. Much research effort is currently focused upon the development of appropriate friction laws and the mechanics using these laws to predict motion along slip surfaces (e.g. References 11, 18 and 19). Considering the development of our contact algorithm, we therefore should use a friction model that is physically realistic and that we can extend in further developments, and as more refined models become available. These criteria are fulfilled using Coulomb's law of friction, with μ_s the static coefficient of friction and μ_d the dynamic (or kinetic) coefficient of friction (Reference 20, pp. 53–64).

Consider the particles initially in contact – those belonging to the target body and those of the contactor. If t_t represents the *developed* tangential tractions along the contact surfaces, we assume that there is no relative motion between two adjacent particles on the contactor and the target in

contact, as long as $|t_t| \leqslant \mu_s t_n$, where t_n is the compressive normal traction (assumed positive). The maximum traction of static friction is the smallest force necessary to start motion. During motion, the magnitude of the tangential traction resisted by friction is $\mu_d t_n$, with $\mu_d \leqslant \mu_s$. The motion continues as long as the frictional traction is developed to equal the dynamic friction $\mu_d t_n$, that can actually be resisted. Once the developed tangential traction drops below the dynamic friction, the relative motion between the contactor and target particles ceases until such time that again the developed tangential traction exceeds the frictional capacity.

We may note that with this friction law, we neglect any elasticity between the particles in contact and assume a rigid plastic contact behaviour. Refinements of this friction law would entail the use of rate and state variables, as discussed for example in Reference 19.

Considering our finite element formulation of the above frictional conditions, we should note the following two important points. First, although rigid plastic behaviour is assumed between particles in contact, the two-dimensional finite element discretization around the contact region can represent nonlinear, e.g. elastic–plastic, material conditions. Secondly, the above friction law is, in our finite element formulation, satisfied in a global sense over each individual contact segment (as discussed in Section 3) consistent with the level of finite element discretization used.

Some preliminaries. For the formulation of our contact solution algorithm we use the incremental procedure—including the notation—presented in Reference 16, Chapter 6, and recognize that for each of the bodies the contact conditions can be imposed by adding to the usual variational indicator, the total potential of the contact forces with the constraint of compatible boundary displacements. Hence, in the formulation we invoke stationarity of the following functional:

$$\Pi_1 = \Pi - \sum_k \mathscr{W}_k \tag{1}$$

where Π is the usual (incremental) total potential leading to the incremental equilibrium equations without contact conditions, and $\sum_k \mathscr{W}_k$ is the incremental potential of the contact forces. This term can be interpreted as a Lagrange multiplier contribution to impose the contact conditions. In the following sections we concentrate on the evaluation of $\mathscr{W}_k$ for a generic node k on the contactor surface (and of the corresponding nodes on the target surface) in sticking and sliding conditions. The values of $\mathscr{W}_k$ and the operations with $\mathscr{W}_k$ are constructed so as to generate the appropriate incremental virtual work equations (hence these could also be derived without reference to a potential).

Assume that, in the incremental solution, the response at time t has been calculated and that $(i-1)$ iterations have been performed to calculate the solution at time $t + \Delta t$. The formulation of the governing equations is achieved by establishing $\mathscr{W}_k$ for the next iteration (i). We repeat that this contribution is the only change in the incremental equilibrium equations presented in Reference 16, Chapter 6.

Figure 2 shows a generic region of contact considered which satisfies the contact conditions. We note that the displacements and co-ordinates are interpolated linearly between adjacent nodes on the contact surfaces of the bodies,† and that some of the nodes can be in contact whereas others are still (or again) in separation. Also, based on the assumptions along the region of contact, the contactor nodes cannot be within the region of the target body, but the target nodes can be inside or outside the contactor body. This point requires particular attention when modelling a problem for use of the contact algorithm.

† Actually, as will become apparent, the contact solution algorithm can also be employed when the contactor and/or target bodies are discretized using parabolic elements (see Sections 4.1 and 4.4).

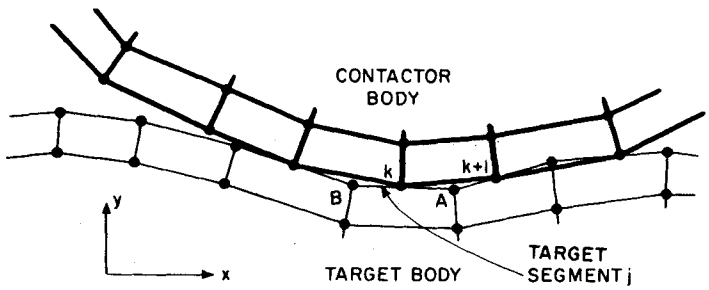

Figure 2. Finite element discretization in contact region. Nodal point numbers on contactor surface increase in direction such that when moving from k to $k+1$ the contactor body is on the left-hand side

2.1 *Potential of contact forces for sticking contact*

A contactor node k is assumed to be in sticking contact under one of two conditions: (a) the contactor node has penetrated the target body in iteration $(i-1)$ whereas it was not in contact after iteration $(i-2)$; (b) the frictional resistance during contact is sufficient to prevent sliding. In case (a) the contact force at node k at the beginning of iteration (i) is zero and the contact force is generated during iteration (i) when the overlap is eliminated.

Figure 3 shows how node k has come into contact with the target segment j formed by nodes A and B, where

$^{t+\Delta t}\mathbf{x}_k^{(i-1)}, {}^{t+\Delta t}\mathbf{x}_A^{(i-1)}, {}^{t+\Delta t}\mathbf{x}_B^{(i-1)}$ = current global co-ordinates of nodes k, A, B, respectively, after iteration $(i-1)$ for the equilibrium configuration corresponding to time $t+\Delta t$.†

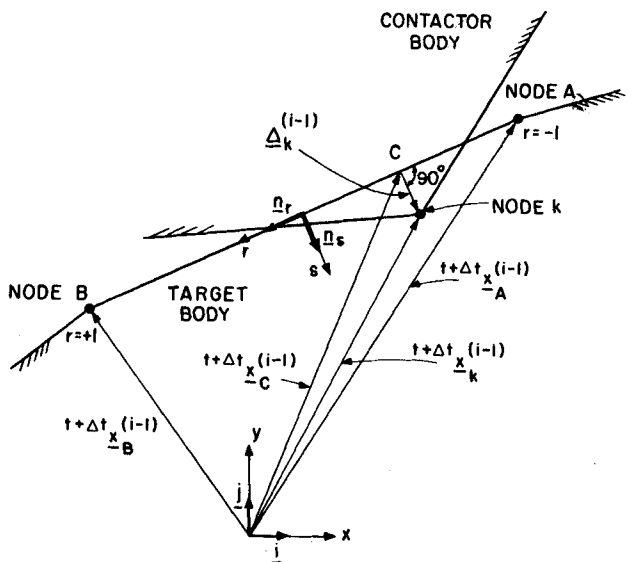

(a) Geometric variables

† Note that, as in Chapter 6 of Reference 16, the left superscript '$t+\Delta t$' on a variable denotes the configuration $t+\Delta t$ in the incremental solution, and does not imply a dynamic analysis (Reference 16, p. 309).

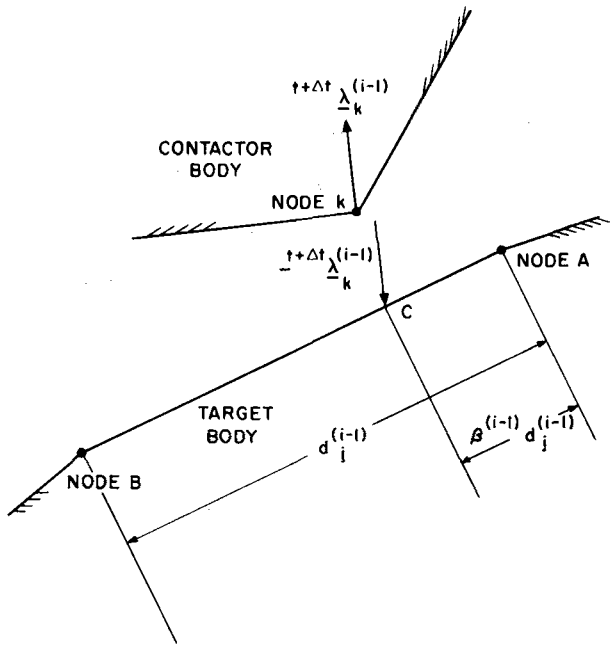

(b) Contact forces

Figure 3. Definition of variables for segment j

$^{t+\Delta t}\mathbf{x}_C^{(i-1)}$ = current global co-ordinates of the assumed physical point of contact of node k.
$\Delta_k^{(i-1)}$ = overlap.
$d_j^{(i-1)}$ = length of segment j.
r, s = local isoparametric co-ordinate system along target surface.
$\mathbf{n}_r, \mathbf{n}_s$ = unit vectors along local axes r, s on target segment, respectively, with respect to the global reference frame; updated during each iteration (but for ease of notation the superscript $(i-1)$ is not given).
$\mathbf{i}, \mathbf{j}$ = unit vectors along global x, y co-ordinate axes.
$\beta^{(i-1)}$ = parameter of location of physical point of contact.

At node k we have a contact force that we denote here as $^{t+\Delta t}\boldsymbol{\lambda}_k^{(i-1)}$, but whose evaluation we discuss in detail in Section 3, where

$$^{t+\Delta t}\boldsymbol{\lambda}_k^{(i-1)} = {}^{t+\Delta t}\lambda_{kx}^{(i-1)}\,\mathbf{i} + {}^{t+\Delta t}\lambda_{ky}^{(i-1)}\,\mathbf{j} \tag{2}$$

Note that the components of $^{t+\Delta t}\boldsymbol{\lambda}_k^{(i-1)}$ appear in the vector $^{t+\Delta t}\mathbf{R}_c^{(i-1)}$ of equation (18). Also, from geometry,

$$\Delta_k^{(i-1)} = {}^{t+\Delta t}\mathbf{x}_k^{(i-1)} - {}^{t+\Delta t}\mathbf{x}_C^{(i-1)} \tag{3}$$

$$d_j^{(i-1)} = \mathbf{n}_r^{\mathrm{T}}\left[{}^{t+\Delta t}\mathbf{x}_B^{(i-1)} - {}^{t+\Delta t}\mathbf{x}_A^{(i-1)}\right] \tag{4}$$

$$\begin{aligned}\beta^{(i-1)} &= \bar{\mathbf{n}}_r^{\mathrm{T}}\left[{}^{t+\Delta t}\mathbf{x}_C^{(i-1)} - {}^{t+\Delta t}\mathbf{x}_A^{(i-1)}\right] \\ &= \bar{\mathbf{n}}_r^{\mathrm{T}}\left[\left({}^{t+\Delta t}\mathbf{x}_k^{(i-1)} - \Delta_k^{(i-1)}\right) - {}^{t+\Delta t}\mathbf{x}_A^{(i-1)}\right]\end{aligned} \tag{5}$$

where

$$\bar{\mathbf{n}}_r = \frac{\mathbf{n}_r}{d_j^{(i-1)}} = \bar{n}_{rx}\mathbf{i} + \bar{n}_{ry}\mathbf{j} \tag{6}$$

And we have for target segment j, the forces equivalent to ${}^{t+\Delta t}\boldsymbol{\lambda}_k^{(i-1)}$,

$${}^{t+\Delta t}\boldsymbol{\lambda}_A^{(i-1)} = -(1-\beta^{(i-1)})\,{}^{t+\Delta t}\boldsymbol{\lambda}_k^{(i-1)} \tag{7}$$

$${}^{t+\Delta t}\boldsymbol{\lambda}_B^{(i-1)} = -\beta^{(i-1)}\,{}^{t+\Delta t}\boldsymbol{\lambda}_k^{(i-1)} \tag{8}$$

Let the displacement increments at nodes k, A, B in iteration (i) be $\Delta\mathbf{u}_k^{(i)}$, $\Delta\mathbf{u}_A^{(i)}$, $\Delta\mathbf{u}_B^{(i)}$, respectively. These displacements are such that the overlap $\Delta_k^{(i-1)}$ is eliminated. Also, if contact was already present, the point of contact C for node k is the same during each iteration, hence $\beta^{(i)} = \beta^{(i-1)}$. The potential $\mathscr{W}_k$ due to the contact force at node k and the corresponding reactions is in iteration i,

$$\mathscr{W}_k = {}^{t+\Delta t}\boldsymbol{\lambda}_k^{(i)\mathrm{T}}(\Delta\mathbf{u}_k^{(i)} + \boldsymbol{\Delta}_k^{(i-1)}) + {}^{t+\Delta t}\boldsymbol{\lambda}_A^{(i)\mathrm{T}}\,\Delta\mathbf{u}_A^{(i)} + {}^{t+\Delta t}\boldsymbol{\lambda}_B^{(i)\mathrm{T}}\,\Delta\mathbf{u}_B^{(i)} \tag{9}$$

Also

$${}^{t+\Delta t}\boldsymbol{\lambda}_k^{(i)} = {}^{t+\Delta t}\boldsymbol{\lambda}_k^{(i-1)} + \Delta\boldsymbol{\lambda}_k^{(i)} \tag{10}$$

where $\Delta\boldsymbol{\lambda}_k^{(i)}$ is the change in the contact force at node k. Using equations (7)–(10) we obtain

$$\begin{aligned}\mathscr{W}_k = {}&{}^{t+\Delta t}\boldsymbol{\lambda}_k^{(i-1)\mathrm{T}}[(\Delta\mathbf{u}_k^{(i)} + \boldsymbol{\Delta}_k^{(i-1)}) - (1-\beta^{(i-1)})\Delta\mathbf{u}_A^{(i)} - \beta^{(i-1)}\Delta\mathbf{u}_B^{(i)}]\\ &+ \Delta\boldsymbol{\lambda}_k^{(i)\mathrm{T}}[(\Delta\mathbf{u}_k^{(i)} + \boldsymbol{\Delta}_k^{(i-1)}) - (1-\beta^{(i-1)})\Delta\mathbf{u}_A^{(i)} - \beta^{(i-1)}\Delta\mathbf{u}_B^{(i)}]\end{aligned} \tag{11}$$

This potential is considered for all contactor nodes k that are in sticking contact.

2.2 *Potential of contact forces for sliding contact*

A contactor node k is assumed to be in sliding contact if, according to the criteria given in Section 3, the tangential force exceeds the frictional capacity. The calculation of total potential for the sliding contact condition is more involved than for sticking contact because the parameter of location, $\beta^{(i-1)}$, changes during iteration (i) to a new value $\beta^{(i)}$. However, the frictional force is assumed to remain constant during the iteration. Using equations (7)–(9) with $\beta^{(i)}$ we have,

$$\mathscr{W}_k = {}^{t+\Delta t}\boldsymbol{\lambda}_k^{(i)\mathrm{T}}[(\Delta\mathbf{u}_k^{(i)} + \boldsymbol{\Delta}_k^{(i-1)}) - (1-\beta^{(i)})\Delta\mathbf{u}_A^{(i)} - \beta^{(i)}\Delta\mathbf{u}_B^{(i)}] \tag{12}$$

where

$$\beta^{(i)} = \beta^{(i-1)} + \Delta\beta^{(i)} \tag{13}$$

and from equation (5) we obtain, by linearization,

$$\Delta\beta^{(i)} \doteq \bar{\mathbf{n}}_r^{\mathrm{T}}[(\Delta\mathbf{u}_k^{(i)} + \boldsymbol{\Delta}_k^{(i-1)}) - (1-\beta^{(i-1)})\Delta\mathbf{u}_A^{(i)} - \beta^{(i-1)}\Delta\mathbf{u}_B^{(i)}] \tag{14}$$

Also, for sliding

$${}^{t+\Delta t}\boldsymbol{\lambda}_k^{(i)} = {}^{t+\Delta t}\boldsymbol{\lambda}_k^{(i-1)} + \Delta\boldsymbol{\lambda}_k^{(i)} \tag{15}$$

$$\Delta\boldsymbol{\lambda}_k^{(i)} = -\Delta\lambda_s^{(i)}\,\mathbf{n}_s \tag{16}$$

where $\Delta\lambda_s^{(i)}$ is the change in the magnitude of the normal component of ${}^{t+\Delta t}\boldsymbol{\lambda}_k^{(i-1)}$. The negative sign in equation (16) is used because an increase in the normal force is acting into the opposite direction of $\mathbf{n}_s$.

Substituting from equations (15) and (16) into equation (12) and assuming $\Delta\beta^{(i)}$ to be negligibly small we obtain

$$\begin{aligned}\mathscr{W}_k = {}&{}^{t+\Delta t}\boldsymbol{\lambda}_k^{(i-1)\mathrm{T}}[(\Delta\mathbf{u}_k^{(i)} + \boldsymbol{\Delta}_k^{(i-1)}) - (1-\beta^{(i-1)})\Delta\mathbf{u}_A^{(i)} - \beta^{(i-1)}\,\Delta\mathbf{u}_B^{(i)}]\\ &+ \Delta\lambda_s^{(i)}\{-\mathbf{n}_s^{\mathrm{T}}[(\Delta\mathbf{u}_k^{(i)} + \boldsymbol{\Delta}_k^{(i-1)}) - (1-\beta^{(i-1)})\Delta\mathbf{u}_A^{(i)} - \beta^{(i-1)}\,\Delta\mathbf{u}_B^{(i)}]\}\end{aligned} \tag{17}$$

This potential is considered for all nodes k that are in sliding contact.

In using equation (17) for $\mathscr{W}_k$ the equilibrium and constraint equations derived below are referred to the contactor nodal point position with $\beta^{(i-1)}$ and correspond to a symmetric coefficient matrix. In practice, $\Delta\beta^{(i)}$ is usually very small (since $\Delta\beta^{(i)}$ reflects the amount of sliding *per iteration*). However, considering equation (17), if desired, it is possible to use $\beta^{(i)}$ instead of $\beta^{(i-1)}$ in the coefficient of ${}^{t+\Delta t}\lambda_k^{(i-1)}$. Then the contact forces corresponding to iteration $(i-1)$ are acting at the segment position with the value $\beta^{(i)}$ whereas the displacement constraint is still referred to the segment position with the value $\beta^{(i-1)}$. Using in this case equation (14) to substitute for $\Delta\beta^{(i)}$, after the derivation of the force vector corresponding to ${}^{t+\Delta t}\lambda_k^{(i-1)}$, a nonsymmetric coefficient matrix is obtained. The use of this gradient matrix would only be warranted if a much improved convergence in the iterations would be achieved.

2.3 *Governing finite element equations*

The incremental finite element equations of motion including contact conditions are generated by substituting from equations (11) and (17) into equation (1) and invoking stationarity, $\delta\Pi_1 = 0$. Hence, we obtain, using the usual procedures

$$\left\{\begin{bmatrix} {}^{t+\Delta t}\mathbf{K}^{(i-1)} & \mathbf{0} \\ \mathbf{0} & \mathbf{0} \end{bmatrix} + [{}^{t+\Delta t}\mathbf{K}_c^{(i-1)}]\right\}\begin{bmatrix} \Delta\mathbf{U}^{(i)} \\ \Delta\boldsymbol{\lambda}^{(i)} \end{bmatrix} = \begin{bmatrix} {}^{t+\Delta t}\mathbf{R} \\ \mathbf{0} \end{bmatrix} - \begin{bmatrix} {}^{t+\Delta t}\mathbf{F}^{(i-1)} \\ \mathbf{0} \end{bmatrix} + \begin{bmatrix} {}^{t+\Delta t}\mathbf{R}_c^{(i-1)} \\ {}^{t+\Delta t}\boldsymbol{\Delta}_c^{(i-1)} \end{bmatrix} \tag{18}$$

where

$\Delta\mathbf{U}^{(i)}$ = vector of incremental displacements in iteration (i); of dimension $(NEQ \times 1)$.
$\Delta\boldsymbol{\lambda}^{(i)}$ = vector of increments in contact forces in iteration (i); $(NEQC \times 1)$.
${}^{t+\Delta t}\mathbf{K}^{(i-1)}$ = usual tangent stiffness matrix including material and geometric nonlinearities after iteration $(i-1)$; $(NEQ \times NEQ)$.
${}^{t+\Delta t}\mathbf{K}_c^{(i-1)}$ = contact stiffness matrix, for the effect of contact conditions after iteration $(i-1)$; $(NEQT \times NEQT)$.
${}^{t+\Delta t}\mathbf{F}^{(i-1)}$ = vector of nodal point forces equivalent to element stresses after iteration $(i-1)$; $(NEQ \times 1)$.
${}^{t+\Delta t}\mathbf{R}$ = vector of total applied external forces at time $t+\Delta t$; $(NEQ \times 1)$.
${}^{t+\Delta t}\mathbf{R}_c^{(i-1)}$ = vector of updated contact forces after iteration $(i-1)$; $(NEQ \times 1)$.
${}^{t+\Delta t}\boldsymbol{\Delta}_c^{(i-1)}$ = vector of overlaps $(NEQC \times 1)$.
NEQ = total number of displacement degrees-of-freedom.
$NEQC$ = total number of incremental contact constraint equations.
= 2 × (total number of nodes in sticking contact) + (total number of nodes in sliding contact).
$NEQT = NEQ + NEQC$.

Each contactor node k contributes to ${}^{t+\Delta t}\mathbf{K}_c^{(i-1)}$, ${}^{t+\Delta t}\mathbf{R}_c^{(i-1)}$ and ${}^{t+\Delta t}\boldsymbol{\Delta}_c^{(i-1)}$. Consider these terms for a single contactor node, since the contributions for a number of nodes are obtained by addition of the individual contributions using the direct stiffness method.[16]

In the case of sticking contact, the first term in equation (11) results in the vector ${}^{t+\Delta t}\mathbf{R}_c^{(i-1)}$, whereas the second term gives the contact stiffness matrix ${}^{t+\Delta t}\mathbf{K}_c^{(i-1)}$ and overlap ${}^{t+\Delta t}\boldsymbol{\Delta}_c^{(i-1)}$,

$${}^{t+\Delta t}\mathbf{R}_c^{(i-1)} = \begin{bmatrix} {}^{t+\Delta t}\lambda_{kx}^{(i-1)} \\ {}^{t+\Delta t}\lambda_{ky}^{(i-1)} \\ -(1-\beta^{(i-1)})\,{}^{t+\Delta t}\lambda_{kx}^{(i-1)} \\ -(1-\beta^{(i-1)})\,{}^{t+\Delta t}\lambda_{ky}^{(i-1)} \\ -\beta^{(i-1)}\;{}^{t+\Delta t}\lambda_{kx}^{(i-1)} \\ -\beta^{(i-1)}\;{}^{t+\Delta t}\lambda_{ky}^{(i-1)} \end{bmatrix} \tag{19}$$

$$ {}^{t+\Delta t}\boldsymbol{\Delta}_c^{(i-1)} = \begin{bmatrix} \Delta_{kx}^{(i-1)} \\ \Delta_{ky}^{(i-1)} \end{bmatrix} \tag{20} $$

$$ {}^{t+\Delta t}\mathbf{K}_c^{(i-1)} = \begin{bmatrix} & & -1 & 0 \\ & & 0 & -1 \\ & & 1-\beta^{(i-1)} & 0 \\ & \mathbf{0} & 0 & 1-\beta^{(i-1)} \\ & & \beta^{(i-1)} & 0 \\ & & 0 & \beta^{(i-1)} \\ \text{symmetric} & & 0 & 0 \\ & & & 0 \end{bmatrix} \tag{21} $$

where the corresponding solution vector is in detail,

$$ \begin{bmatrix} \Delta\mathbf{U}^{(i)} \\ \Delta\boldsymbol{\lambda}^{(i)} \end{bmatrix} = \begin{bmatrix} \Delta\mathbf{u}_k^{(i)} \\ \Delta\mathbf{u}_A^{(i)} \\ \Delta\mathbf{u}_B^{(i)} \\ \Delta\lambda_k^{(i)} \end{bmatrix} \tag{22} $$

In the case of sliding contact, we proceed in much the same way to obtain, using equation (17), again the vector ${}^{t+\Delta t}\mathbf{R}_c^{(i-1)}$ in equation (19) and a matrix ${}^{t+\Delta t}\mathbf{K}_c^{(i-1)}$ resembling the matrix in equation (21) but with only one constraint equation. Also,

$$ {}^{t+\Delta t}\boldsymbol{\Delta}_c^{(i-1)} = [-n_{sx}\ \Lambda_{kx}^{(i-1)} - n_{sy}\Delta_{ky}^{(i-1)}] \tag{23} $$

and the corresponding solution vector is

$$ \begin{bmatrix} \Delta\mathbf{U}^{(i)} \\ \Delta\lambda^{(i)} \end{bmatrix} = \begin{bmatrix} \Delta\mathbf{u}_k^{(i)} \\ \Delta\mathbf{u}_A^{(i)} \\ \Delta\mathbf{u}_B^{(i)} \\ \Delta\lambda_s^{(i)} \end{bmatrix} \tag{24} $$

Although we have simply listed the vector ${}^{t+\Delta t}\mathbf{R}_c^{(i-1)}$ as shown in equation (19), an important ingredient of our algorithm is that the actual elements of this force vector are derived as explained in the next section.

Note that the above equations (used for the sample solutions in Section 4) correspond to a full Newton iteration. Our experiences with the solution of contact problems have so far shown that for the contact equations full Newton–Raphson iteration is usually best.

3 EVALUATION OF STICKING AND SLIDING CONDITIONS, AND FRICTIONAL RESISTANCE

Much of the difficulty of solving contact problems lies in the design of appropriate procedures for numerically updating the contact conditions at a contactor node. In other words, the algorithm has to decide whether a node is not in contact and whether the matrices for sticking contact or the matrices for sliding contact shall be included in the system of equations. Appropriate decisions during the iteration concerning these conditions are most important for a reliable and effective scheme.

After iteration $(i-1)$ the nodal point displacements ${}^{t+\Delta t}\mathbf{U}^{(i-1)}$ and nodal point forces $\Delta\mathbf{R}^{(i-1)}$ are known where (see Figure 4)

$$ \Delta\mathbf{R}^{(i-1)} = {}^{t+\Delta t}\mathbf{F}^{(i-1)} - {}^{t+\Delta t}\mathbf{R} \tag{25} $$

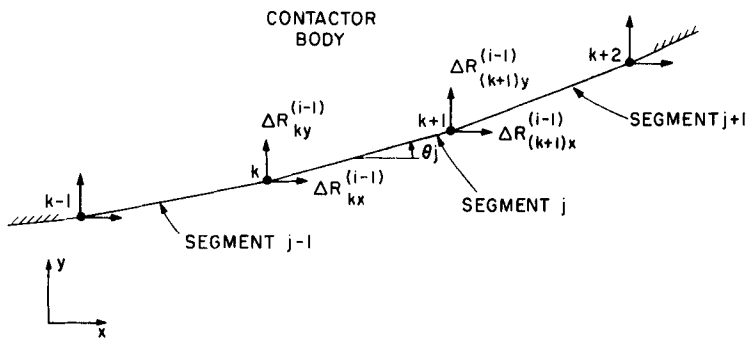

(a) Forces acting onto contactor body

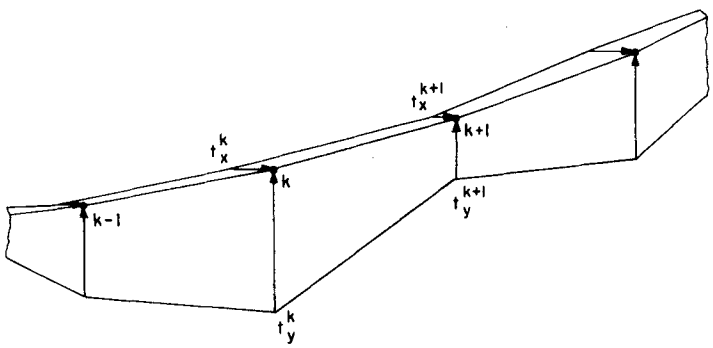

(b) Tractions acting onto contactor body

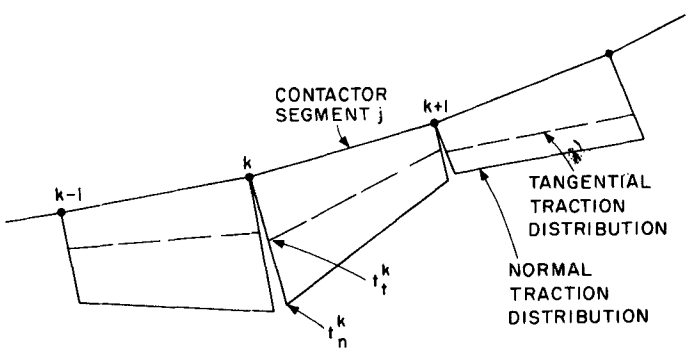

(c) Normal and tangential tractions on contactor body. Normal traction is positive when acting onto the body; tangential traction is positive when acting from node k to node $(k+1)$

Figure 4. Calculation of normal and tangential tractions on contactor body for evaluation of contact forces

We note that at the nodes not belonging to a contact surface the components of $\Delta\mathbf{R}^{(i-1)}$ are (minus) the out-of-balance loads usually encountered in nonlinear analysis,[16] but corresponding to the boundary nodes affected by the contact, the contact forces ${}^{t+\Delta t}\mathbf{R}_c^{(i-1)}$ are active. These forces are evaluated from the loads $\Delta\mathbf{R}^{(i-1)}$ and correspond to tension release, sticking or sliding conditions.

The procedure of calculating the contact forces from the vector $\Delta\mathbf{R}^{(i-1)}$ is effective because an incrementation of the Lagrange multipliers used in equation (18) can — in other than geometrically

and materially linear analyses of sticking contact conditions—lead to serious errors of linearization.

In the following we consider the contactor segments and contactor nodes, and we discuss how the conditions of node sticking and sliding can be reached, and how the contact forces ${}^{t+\Delta t}\mathbf{R}_c^{(i-1)}$ are evaluated.

When a contactor node penetrates the target body in an iteration, which is decided kinematically by the displacements of the contactor and target bodies leading to a geometric overlap (see Figure 3), the matrices in equations (19)–(22) are included in the solution for the next incremental displacements. Hence, in the first iteration from no contact to a contact condition, sticking is assumed.† This is the mechanism used to evaluate the nodal point forces and enable a decision on whether sticking or sliding conditions are really applicable.

3.1 *Contactor segment distributed tractions and resultant forces*

The decision on whether a contactor node is releasing or is in sticking or sliding conditions is perhaps most quickly based on considering the total and relative magnitudes of the calculated nodal point forces. However, this can lead to some numerical difficulties, and it is deemed more effective to establish the condition at a contactor node from the accumulated effects and conditions of the contactor segments adjacent to the node.

The first step in our procedure is to calculate the distribution of the tractions along the contactor boundary given the nodal point forces $\Delta\mathbf{R}^{(i-1)}$. Let t_x^k and t_y^k be the magnitudes of the distributed tractions (force/unit area) at the nodal point k (see Figure 4), then we have with a linear displacement interpolation in a 'consistent' approach to calculate the tractions from the nodal point forces, in plane stress and plane strain analyses, with uniform thickness h,‡

$$\begin{bmatrix} \Delta R_{kx}^{(i-1)} \\ \Delta R_{ky}^{(i-1)} \end{bmatrix} = h \begin{bmatrix} t_x^{k-1} & t_x^k & t_x^{k+1} \\ t_y^{k-1} & t_y^k & t_y^{k+1} \end{bmatrix} \begin{bmatrix} \dfrac{d_{j-1}^{(i-1)}}{6} \\ \dfrac{d_{j-1}^{(i-1)} + d_j^{(i-1)}}{3} \\ \dfrac{d_j^{(i-1)}}{6} \end{bmatrix} \tag{26}$$

and in axisymmetric analysis (assuming the y-axis to be the axis of revolution)

$$\begin{bmatrix} \Delta R_{kx}^{(i-1)} \\ \Delta R_{ky}^{(i-1)} \end{bmatrix} = \begin{bmatrix} t_x^{k-1} & t_x^k & t_x^{k+1} \\ t_y^{k-1} & t_y^k & t_y^{k+1} \end{bmatrix} \begin{bmatrix} \dfrac{d_{j-1}^{(i-1)}}{12}({}^{t+\Delta t}x_{k-1}^{(i-1)} + {}^{t+\Delta t}x_k^{(i-1)}) \\ \dfrac{d_{j-1}^{(i-1)}}{12}({}^{t+\Delta t}x_{k-1}^{(i-1)} + 3^{t+\Delta t}x_k^{(i-1)}) + \dfrac{d_j^{(i-1)}}{12}(3^{t+\Delta t}x_k^{(i-1)} + {}^{t+\Delta t}x_{k+1}^{(i-1)}) \\ \dfrac{d_j^{(i-1)}}{12}({}^{t+\Delta t}x_k^{(i-1)} + {}^{t+\Delta t}x_{k+1}^{(i-1)}) \end{bmatrix} \tag{27}$$

† We may note that for the special case of frictionless contact, i.e. $\mu_s = \mu_d = 0{\cdot}0$, we can directly assume perfect sliding conditions.

‡ Instead of using the consistent traction recovery given here, it would also be possible to employ a lumped approach.

where ${}^{t+\Delta t}x_k^{(i-1)}$ is the x-co-ordinate of nodal point k at the end of iteration $(i-1)$. Using equations (26) and (27) a tridiagonal coefficient matrix is established that relates the unknown tractions to the known values of $\Delta\mathbf{R}^{(i-1)}$, and the equations can be solved to calculate, in each iteration, the nodal values t_x^k and t_y^k for all nodes in contact. These values are then employed to evaluate the tangential and normal segment tractions, t_t^k and t_n^k, at the nodes. Note that to evaluate these tractions for segment j, the values t_x^k, t_y^k and t_x^{k+1}, t_y^{k+1} are simply transformed to the tangential and normal directions defined by the angle θ_j of the segment. This results in general into a discontinuity of the normal and tangential segment tractions at the nodal points, see Figure 4.

For the definition of the state of a segment, we need the total normal and tangential forces applied to the segment. In the case of plane stress and plane strain analyses, the total resultant normal force, T_n^j, acting on segment j is

$$T_n^j = h\frac{d_j^{(i-1)}}{2}(t_n^k + t_n^{k+1}) \tag{28}$$

and the total resultant tangential force, T_t^j, acting on segment j is

$$T_t^j = h\frac{d_j^{(i-1)}}{2}(t_t^k + t_t^{k+1}) \tag{29}$$

where $d_j^{(i-1)}$ is the length of the contactor segment j in iteration (i). Similarly, for axisymmetric analysis we have

$$T_n^j = \frac{d_j^{(i-1)}}{6}\{2({}^{t+\Delta t}x_k^{(i-1)}\ t_n^k + {}^{t+\Delta t}x_{k+1}^{(i-1)}\ t_n^{k+1}) + ({}^{t+\Delta t}x_{k+1}^{(i-1)}\ t_n^k + {}^{t+\Delta t}x_k^{(i-1)}\ t_n^{k+1})\} \tag{30}$$

and

$$T_t^j = \frac{d_j^{(i-1)}}{6}\{2({}^{t+\Delta t}x_k^{(i-1)}\ t_t^k + {}^{t+\Delta t}x_{k+1}^{(i-1)}\ t_t^{k+1}) + ({}^{t+\Delta t}x_{k+1}^{(i-1)}\ t_t^k + {}^{t+\Delta t}x_k^{(i-1)}\ t_t^{k+1})\} \tag{31}$$

With the above calculations completed the algorithm decides on the state of the segment using the segment resultant forces T_n^j, T_t^j and Coulomb's law of friction globally applied over the segment.

3.2 *Segment release*

The segment is assumed to have experienced tension release if T_n^j is negative, and in this case the contactor segment normal and tangential tractions are set to zero.

3.3 *Assume segment was in previous iteration in sticking contact*

Using the total normal force on the segment T_n^j the frictional capacity of the segment T_f^j is calculated using Coulomb's law of friction, $T_f^j = \mu_s T_n^j$, where μ_s for the segment is set equal to μ_d if the segment was ever in sliding (see Section 4.2). The following two situations can now arise.

Case 1. The frictional capacity of the segment is larger than the applied total tangential force, i.e. $T_f^j \geq |T_t^j|$. The segment continues to stick.

Case 2. The frictional capacity of the segment is smaller than the applied total tangential force, i.e. $T_f^j < |T_t^j|$. The state of the segment is now updated to sliding, with $T_f^j = \mu_d T_n^j$.

The results on whether the segment continues to stick or is now sliding are later used in deciding whether the contactor nodes are sticking or sliding (see Section 3.5).

Aside from deciding on the sticking and sliding conditions of the segments, the contributions to the vector ${}^{t+\Delta t}\mathbf{R}_c^{(i-1)}$ must also be evaluated. This is done differently in the above two situations.

In Case 1 the distributed tangential and normal tractions on the segment j are employed to calculate the nodal point consistent loads, see Figure 5. We note that if also the conditions of the adjacent segments $(j-1)$ and $(j+1)$ correspond to Case 1, these nodal point consistent loads are at the nodes k and $k+1$ simply the values in $\Delta\mathbf{R}^{(i)}$.

In Case 2 the segment is sliding, and Figure 5(b) summarizes the tractions t_t used in the calculation of ${}^{t+\Delta t}\mathbf{R}_c^{(i-1)}$. Note that a uniform traction is assigned such that in sliding conditions the total tangential force is scaled down to equal the frictional capacity. Using a uniform frictional traction represents perhaps the simplest way of globally satisfying Coulomb's law of friction over the segment.† Figure 5 shows the tractions used in plane stress and plane strain analyses; in axisymmetric solution the value $(t_t^k + t_t^{k+1})/2$ of Figure 5 is replaced by $\bar{t}_t$,

$$\bar{t}_t = \frac{2T_t^j}{d_j^{(i-1)}({}^{t+\Delta t}x_k^{(i-1)} + {}^{t+\Delta t}x_{k+1}^{(i-1)})} \tag{32}$$

In summary, unless there is tension release (see Section 3.2) the contact forces ${}^{t+\Delta t}\mathbf{R}_c^{(i-1)}$ are calculated as the consistent nodal point loads corresponding to the tangential tractions t_t, shown in Figure 5, and the unaltered normal tractions shown in Figure 4. In tension release, both the normal and tangential tractions on the segment are set to zero.

3.4 *Assume segment was in previous iteration in sliding contact*

If the segment was in sliding contact, analogous calculations to those described in Section 3.3 are performed, but the friction coefficient used is μ_d. Hence, in Case 1 the segment changes to sticking, whereas in Case 2 the segment continues to slide.

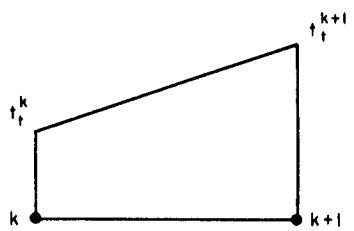

(a) Case 1

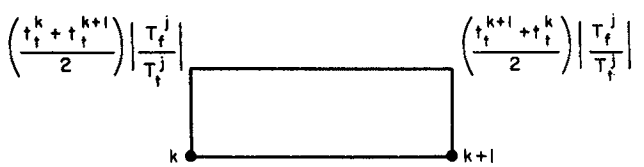

(b) Case 2

Figure 5. Tangential tractions used in calculation of contact force vector ${}^{t+\Delta t}\mathbf{R}_c^{(i-1)}$; in axisymmetric analysis replace $(t_t^k + t_t^{k+1})/2$ by $\bar{t}_t$ of equation (32)

†Updating the tangential tractions in this way raises questions on the convergence of the iterative solution, as studied in a forthcoming communication.

Table I. State of contactor node as decided by states of adjoining segments

State of adjoining segments		
One adjoining segment	Other adjoining segment	State of node
Sticking	Sticking	Sticking
	Sliding	
	Tension release	
Sliding	Sliding	Sliding
	Tension release	
Tension release	Tension release	Tension release

3.5 *Conditions of contactor nodes*

Once the conditions of the contactor segments have been decided as discussed above, the algorithm determines the conditions of the nodes on the contactor surface. Table I summarizes how the various conditions (release, sticking and sliding) of a contactor node are reached. We may note that these conditions decide on whether zero (corresponding to no contact or contact release), one (corresponding to sliding) or two (corresponding to sticking) contact equations are to be included in the incremental equations for each contactor node.

The decision on whether a contactor node k is not in contact, or is in sliding or sticking contact, and the evaluation of the contact matrices and the contact forces to be used in equation (18) gives all the ingredients to proceed with the iteration (i).

4 SOME SAMPLE SOLUTIONS

The algorithm presented in the previous sections was implemented in ADINA and in the following we present the results of some sample analyses. In these analyses, the primary objective was to study the performance of the algorithm in order to identify where improvements are needed rather than to solve actual practical problems.

It is our experience that regarding the solution of contact problems some 'very simple looking' problems, including frictional conditions and the elasticity of the structure, may provide quite severe tests on the performance of an algorithm, and in fact may be more difficult to solve than actual practical engineering problems.

4.1 *Analyses of Hertz contact problems*

Figure 6 shows the contact problem considered and the finite element idealization used. In this problem a long cylinder with radius $R = 10$ was analysed; hence, in the model, plane strain conditions were assumed. The rigid target surface was modelled by specifying nodes with no degrees-of-freedom. In the region of anticipated contact, 8-node elements were used to model the contactor with one contactor segment always spanning over one 8-node element side, and these elements were modelled as materially-nonlinear-only or using the total Lagrangian formulation.[16] To simulate the load application, the vertical displacements were prescribed along the top surface of the model and the total load P for a prescribed displacement was calculated by integrating the contact pressures. Figure 7 gives the calculated contact pressures and a comparison with the Hertz analytical solution.[21]

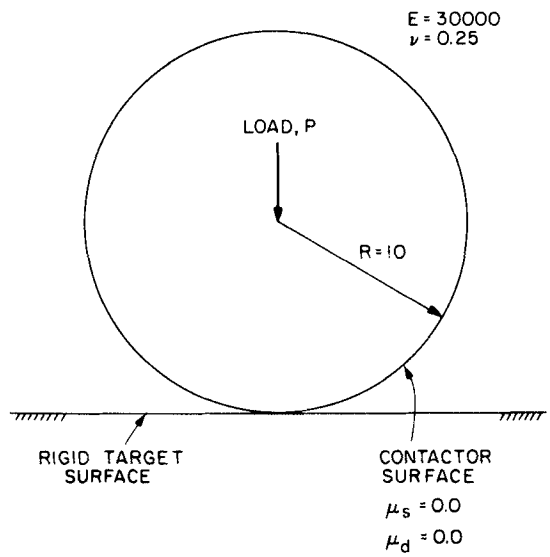

(a) Problem considered

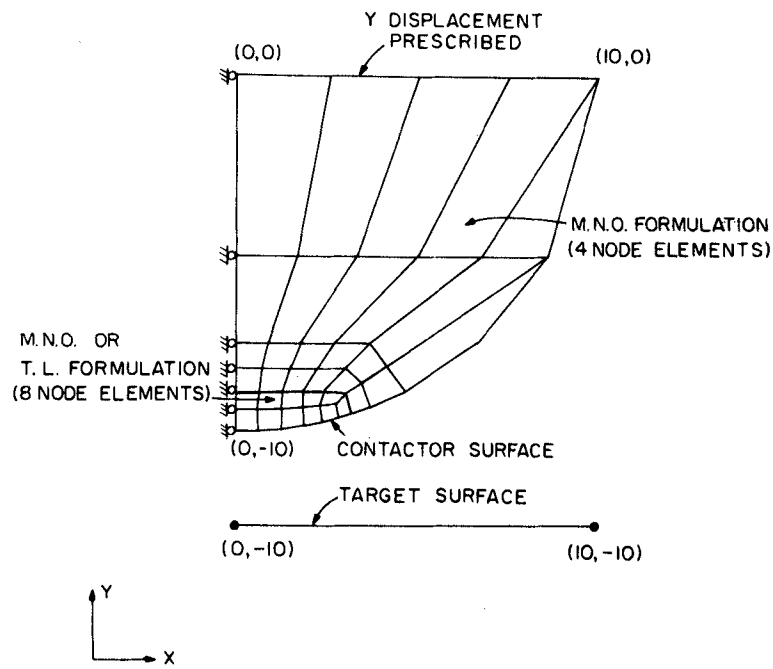

(b) Finite element mesh used; long cylinder is modelled

Figure 6. Analysis of Hertz plane strain contact problem (M.N.O. and T.L. formulations denote materially-nonlinear-only and total Lagrangian formulations, respectively[16])

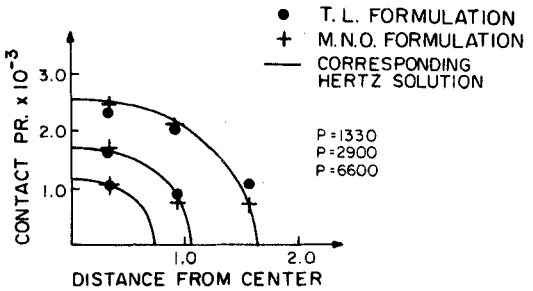

Figure 7. Solution to the plane strain Hertz problem

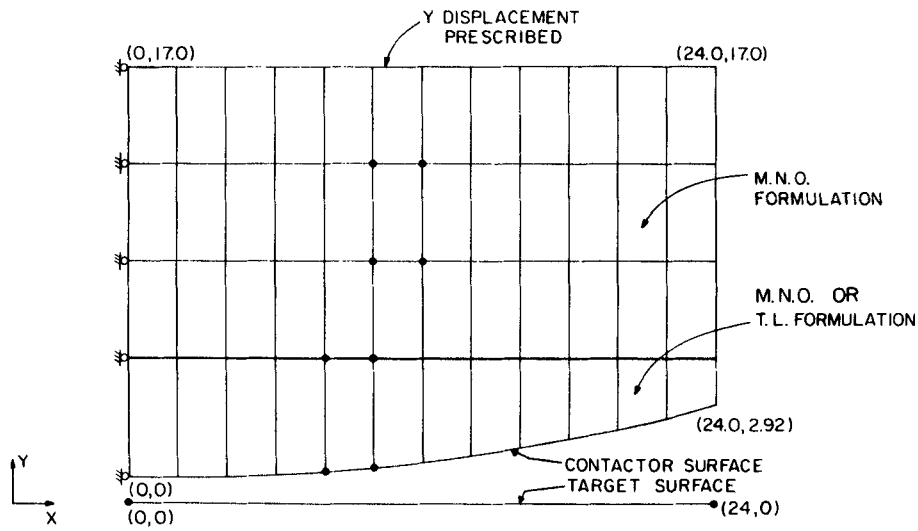

Figure 8. Analysis of Hertz axisymmetric contact problem

We may note that only a few solution points are given in Figure 7, because the program outputs the mean traction over a segment and at the maximum applied load ($P = 6600$) only three segments were in contact. In order to obtain more finite element solution points and a higher solution accuracy, a finer finite element discretization on the contactor surface is required.

Next, the Hertz contact problem of a sphere of radius $R = 100$ was analysed. Hence, Figure 6(a) still shows the contact problem, but now $R = 100{\cdot}0$ and axisymmetric conditions are considered. Figure 8 gives the finite element mesh used in this analysis and Figure 9 shows the calculated contact pressures and a comparison with the Hertz solution.

4.2 *Motion of a rubber sheet in a converging channel*

A sheet of rubber in plane stress was confined to move in a rigid horizontal channel. Figure 10 shows the sheet and the finite element idealization used.† The right face of the sheet was subjected to

† Note that the rigid target surface was modelled using 12 segments for the sole purpose of demonstrating that contactor nodes can slide over target nodes.

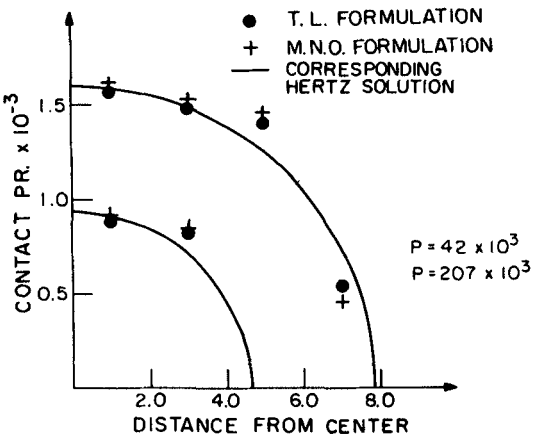

Figure 9. Solution to the axisymmetric Hertz problem

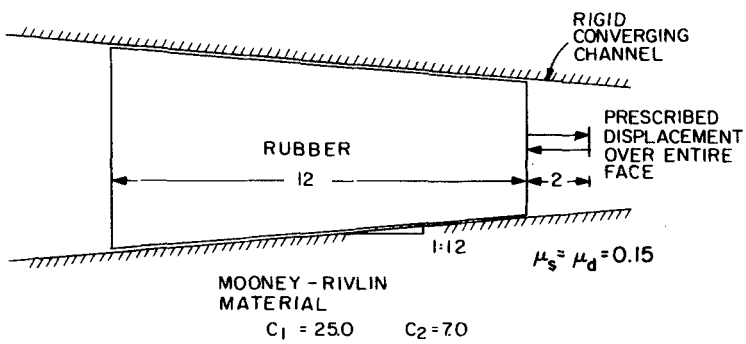

(a) Problem considered

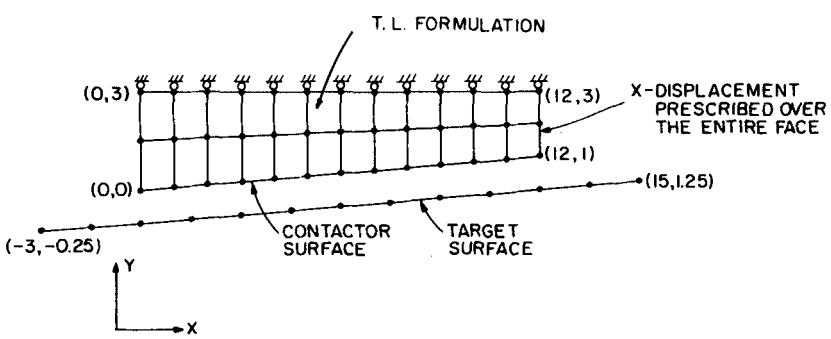

(b) Finite element mesh used

Figure 10. Analysis of motion of a rubber sheet in a converging channel

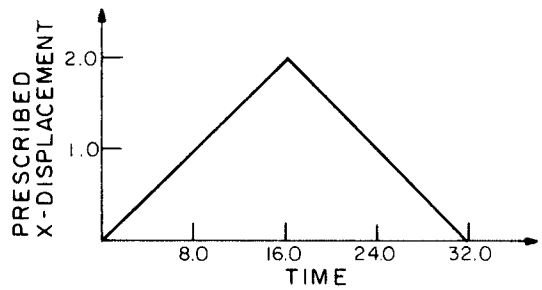

Figure 11. Prescribed displacements in analysis of rubber sheet, time step $\Delta t = 0{\cdot}5$

the displacement history given in Figure 11, making this a large deformation problem. Note that the displacements were assumed to vary slowly so that inertia effects could be neglected.

Although the solution obtained could not be compared with an available solution, this is an interesting problem to study the performance of the contact algorithm. Also, the essential features and solution difficulties of this problem are frequently encountered in actual practical problems; e.g. analysis of metal forming processes.

Figure 12 shows the distribution of normal and tangential tractions for different load steps in the solution. The tractions close to the face at which the displacements are imposed are not shown, because a fine finite element idealization would be required to obtain good stress predictions near the face. Note that the magnitudes of the tangential tractions, t_t, for times 8, 14 and 24 are essentially equal to μ_d times t_n—because practically the entire rubber sheet is sliding through the channel—and that the tangential tractions at time 24 are acting in the opposite direction to the tractions at times 8 and 14. However, at time 18 the tangential tractions have only partially reversed and some segments are still in sticking conditions. It is this change in tangential tractions, resulting from the reversal in motion, that is quite difficult to analyse.

Figure 12 also shows the results obtained when assuming a frictionless motion. As expected, for the frictionless case the normal tractions are significantly larger at times 8 and 14 (the imposed displacements increase) and smaller at times 18 and 24 (the imposed displacements decrease), when compared with the results including friction.

Finally, the motion of the rubber sheet for $\mu_s > \mu_d$ was also analysed ($\mu_s = 0{\cdot}20$, $\mu_d = 0{\cdot}15$). For this case, two different solution algorithms were employed. In the first solution our usual algorithm was used, in which the value of μ_s for a segment was set equal to μ_d as soon as, and for all times thereafter, the static frictional resistance was exceeded for the segment. Since the effect of $\mu_s > \mu_d$ is then a transient phenomenon, the solution results for the times considered in Figure 12 are (very closely) the same as the results obtained for the case $\mu_s = \mu_d$. In the second analysis, as an experiment, the value of $\mu_s = 0{\cdot}20$ was kept throughout the solution and the results marked $\mu_s = 0{\cdot}20$, $\mu_d = 0{\cdot}15$ in Figure 12 were obtained. It should be noted that in this analysis the time step used ($\Delta t = 0{\cdot}5$) is an important (physical) variable of the problem—because the solution procedure simulates the frictional motion of the sheet for each solution step separately—and it is questionable whether the assumptions used in this numerical solution appropriately simulate the actual physical process of motion. However, it is interesting to note that for the chosen values of μ_s and μ_d relatively small differences in the tractions were calculated when compared with the solution for $\mu_s = \mu_d$ (except for the tangential tractions at time 18 which more drastically changed sign when $\mu_s > \mu_d$). It should be emphasized that these solutions of the rubber sheet when $\mu_s > \mu_d$ should only

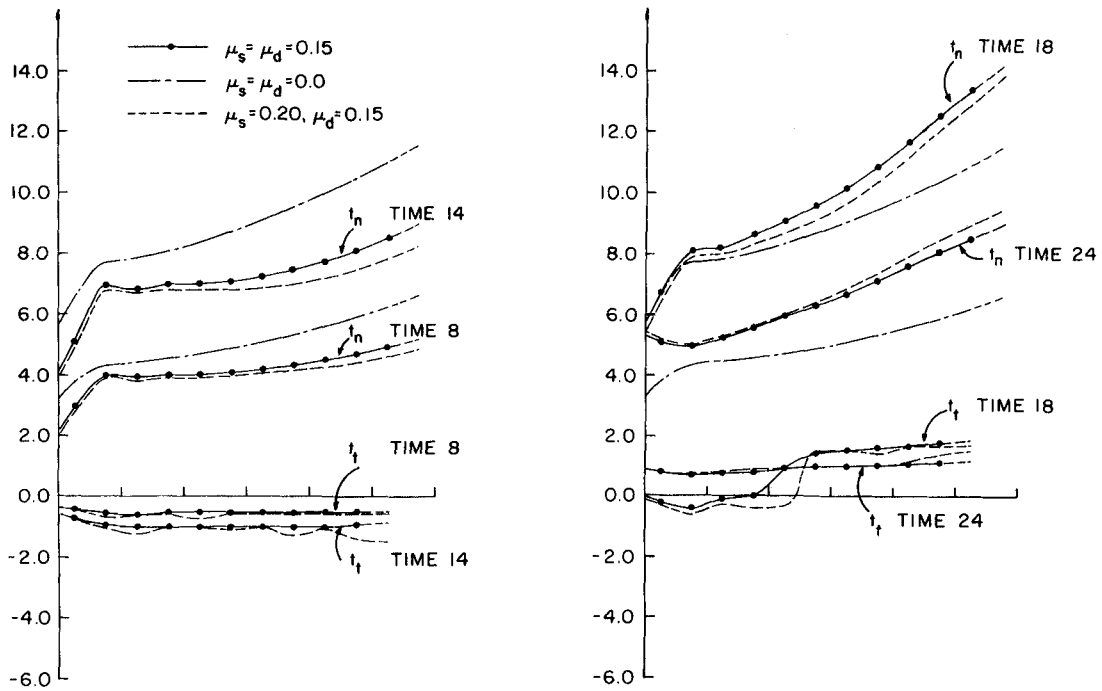

(a) At times 8 and 14

(b) At times 18 and 24

Figure 12. Distributed tractions in analysis of rubber sheet moving through rigid channel (solid line refers to the solution for $\mu_s = \mu_d$ and the solution for $\mu_s > \mu_d$ using our usual algorithm; dashed line refers to 'experiment' when $\mu_s > \mu_d$)

be regarded as a rather brief numerical experiment, because there are many difficult questions related to the physics, and to our numerical analysis procedure, for this problem that need much further study.[19]

4.3 *Analysis of a snapped wire in continuous wiring*

The practical application of this problem lies in the analysis of the conditions that arise when a wire of a continuous wiring around a cylinder snaps.

Figure 13 shows the model considered. Note that the snapped wire is free of constraints at $x = 0$ (for $y \geqslant 0$). The objective was to calculate the stress distribution in the continuous wiring (modelled here as a continuum) at the maximum load application, $\sigma_{yy} = 300$ MPa and $\sigma_{xx} = 750$ MPa.

Figure 13(b) shows the finite element idealization used for the analysis and Figure 14 gives some calculated stresses and a comparison with the results obtained by Boman.[22] The solution with our contact algorithm was obtained using one load step to apply the initial stress σ_{yy} and then two load steps with $\Delta t = 1{\cdot}0$, as shown in Figure 13(a), to reach the final stress condition.

4.4 *Analysis of a buried pipe*

Frictional conditions must frequently be modelled in the analysis of soil–structure interactions.[15,23]

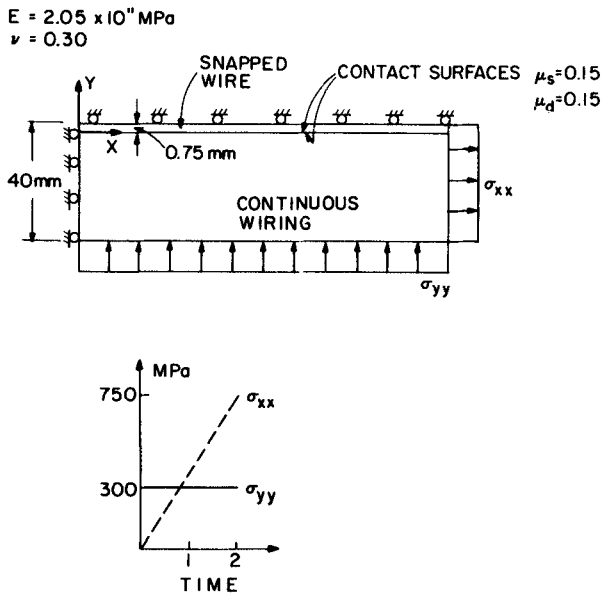

(a) Problem considered; time step $\Delta t = 1{\cdot}0$

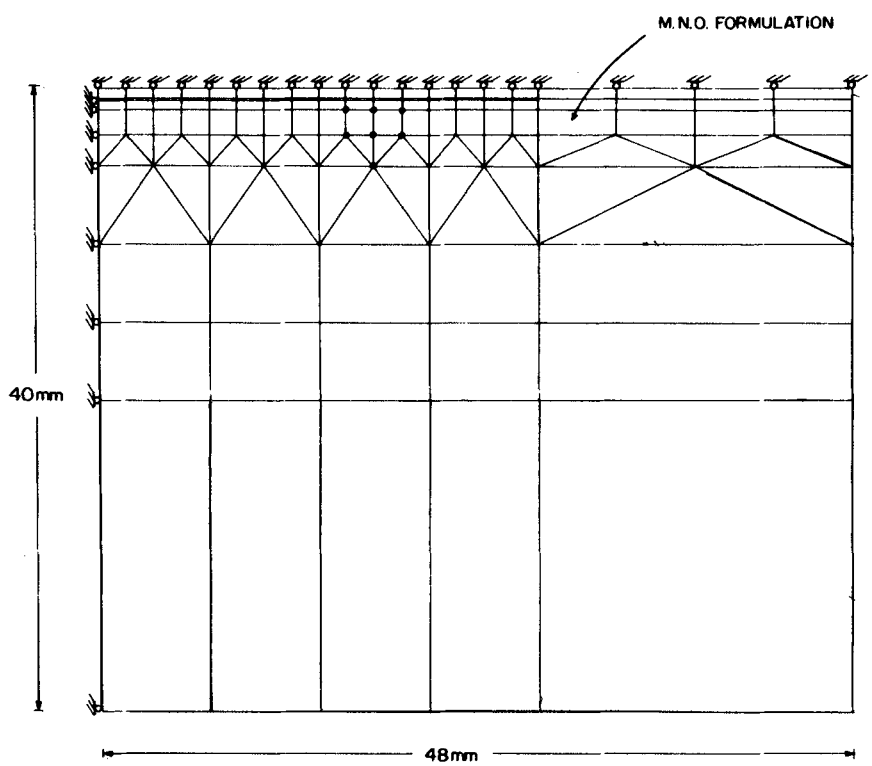

(b) Finite element mesh used

Figure 13. Analysis of wiring around cylinder

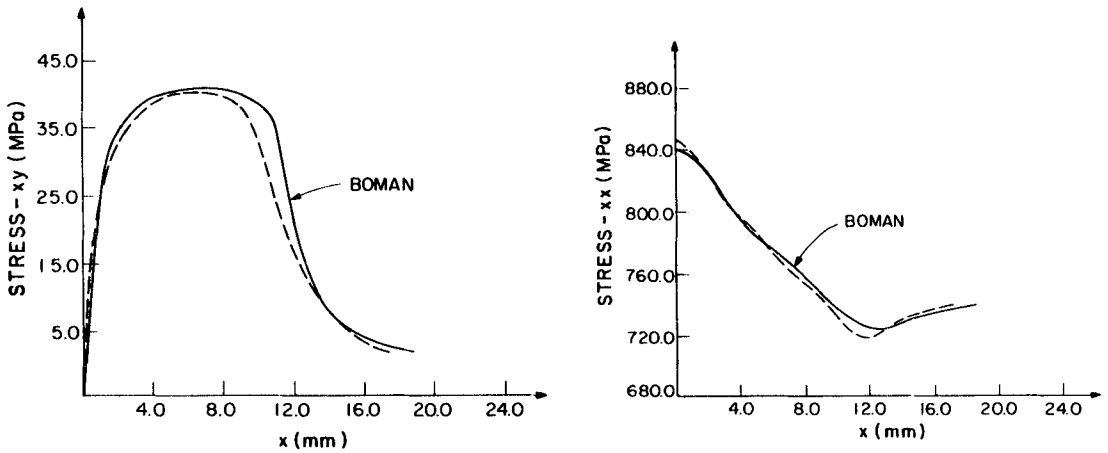

Figure 14. Stresses just below contact surfaces in analysis of wiring around cylinder

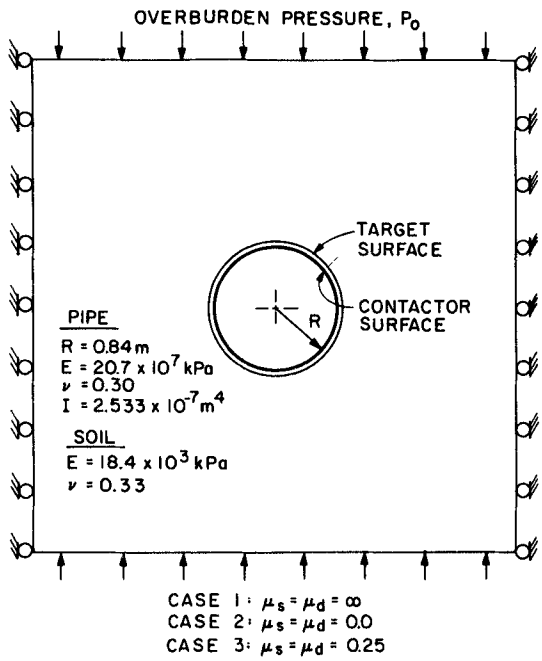

Figure 15. Pipe buried in soil subjected to overburden pressure $P_0 = 100\,\text{kPa}$, $\mu = \mu_s = \mu_d$

Figure 15 shows a pipe buried in soil subjected to the overburden pressure $P_0 = 100$ kPa. The objective of the analysis was to predict the tractions along the pipe–soil interface. In this analysis, both the pipe and the soil were considered linear elastic media, although in practice the soil may need to be considered nonlinear.

Figure 16 shows the finite element idealization used for the analysis, and Figure 17 gives the

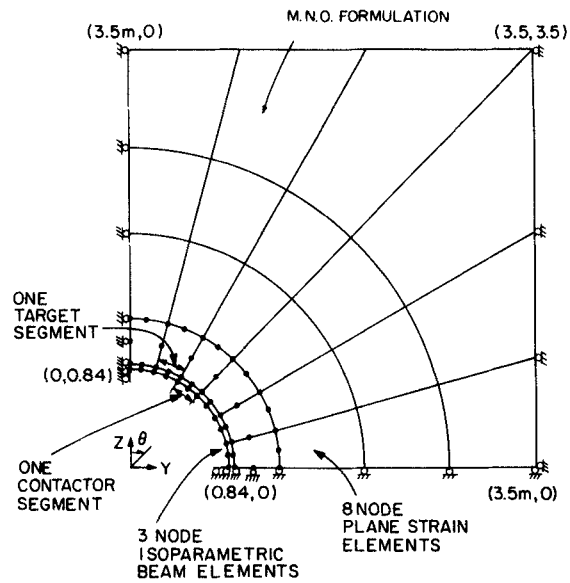

Figure 16. Finite element idealization used for analysis of buried pipe

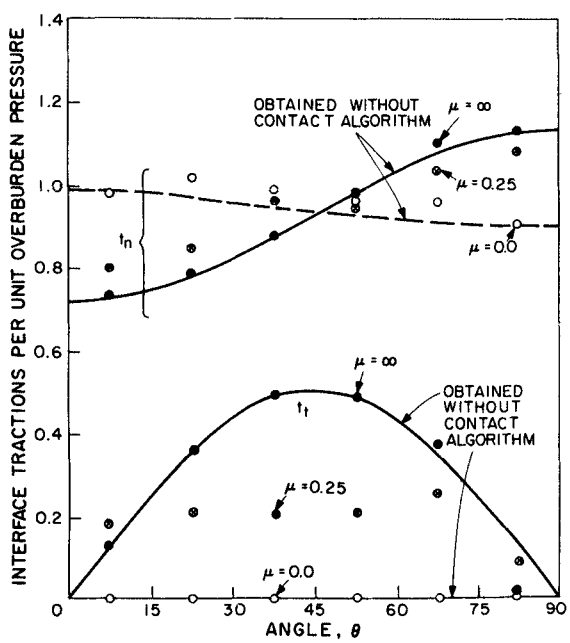

Figure 17. Predicted tractions on pipe–soil interface; solution obtained using four load increments of equal size

predicted tractions along the contact surface.† Also shown in Figure 17 are the tractions along the interface for the friction coefficients $\mu = 0{\cdot}0$ and $\mu = \infty$ calculated without the use of the contact algorithm. These results have been obtained by simply using constraint equations so that the pipe and soil nodal displacements are the same perpendicular to the pipe surface, and free tangentially when $\mu = 0{\cdot}0$ and the same tangentially when $\mu = \infty$.

Figure 17 shows that the results using the contact algorithm are slightly different from those obtained without the contact algorithm. These differences arise mainly because of the traction recovery used in the contact algorithm, and because the contact algorithm always uses the updated nodal point positions (including the displacements) for the contact force calculations, whereas these deformations were neglected when using the constraint equations.

5 CONCLUSIONS

An algorithm for the solution of two-dimensional contact problems, including large deformation and frictional conditions, has been presented. The solution procedure uses a Lagrange multiplier technique to incrementally impose the deformation constraints along the contact surfaces. The contact forces are evaluated from distributed tractions that act on the contactors. The tractions are calculated from the nodal point forces (which correspond to the internal element stresses and the externally applied loading) and the frictional conditions based on Coulomb's law. The solution results obtained using the algorithm in some contact problems have been presented to demonstrate some of the features of the solution procedure.

Considering the way frictional conditions are accounted for in the algorithm, some important assumptions are used. First, the frictional forces in sliding are assumed to act in the same directions as the contact tangential forces prior to sliding. This assumption may require relatively small load increments in the solution. Second, the frictional calculations make only use of the total tangential and normal forces acting on the segments, and do not account for the variation of the tractions over the segments. And third, the relatively simple friction law of Coulomb is employed. A more refined friction law would include rate and state-dependent factors. Using Coulomb's friction law with $\mu_s = \mu_d$ already a large number of contact problems can be modelled using our algorithm, but various questions relating to the physics of motion, and to our numerical solution procedure, must still be addressed when $\mu_s > \mu_d$.[19]

In this first paper, we have concentrated on presenting the theory used and on indicating some applications. Our experiences with the algorithm have been most encouraging, but the field of analysis of contact problems is very large, and many most interesting aspects relating to our algorithm deserve further studies, such as:

1. The effect of the finite element mesh used for a problem on the performance of the solution procedure.
2. Effective modelling of the target and contactor bodies, with respect to selection of an appropriate number of contactor and target segments for determination of contact.
3. The use of appropriate load incrementation for solution of specific problems, and the effect of different sequences of load application, in particular when $\mu_s > \mu_d$.
4. The choice of iteration procedure and convergence criteria (for example, perhaps more effective methods than full Newton iteration can be identified).
5. The use of different coefficient matrices that include non-symmetric parts in the gradient.
6. The use of a lumped approach for the traction recovery instead of the consistent approach, and the use of higher order contact segments.

† As seen in the figure, the case $\mu = \infty$ can be modelled with the contact algorithm using any large value of μ.

7. Rigorous mathematical analyses and convergence studies of the algorithm for frictional conditions.

These studies would be very valuable because they will yield further insight into the solution procedure and provide the basis for improvements of the solution method. We are currently pursuing such studies and plan to report upon them in future communications.

ACKNOWLEDGEMENTS

We are grateful for the financial support provided by the U.S. Army Contract No. DAAK11-82-K-0015 and by the ADINA users group for this work. We also would like to thank J. T. Oden of the University of Texas, Austin, for stimulating discussions regarding this research.

REFERENCES

1. C. H. Chan and I. S. Tuba, 'A finite element method for contact problems of solid bodies', *Int. J. Mech. Sci.*, **13** (1971).
2. R. E. Goodman, R. L. Taylor and T. L. Brekke, 'A model for the mechanics of jointed rock', *J. Soil Mech. Found. Div.*, ASCE, **94** (SM3), 637–659 (1968).
3. E. A. Wilson and B. Parsons, 'Finite element analysis of elastic contact problems using differential displacements', *Int. j. numer. methods eng.*, **2**, 387–395 (1970).
4. A. Francavilla and O. C. Zienkiewicz, 'A note on numerical computation of elastic contact problems', *Int. j. numer. methods eng.*, **9**, 913–924 (1975).
5. H. S. Cheng and L. M. Keer (Eds.), *Solid Contact and Lubrication*, AMD-Vol. 39, American Society of Mechanical Engineers, 1980.
6. T. J. R. Hughes, R. L. Taylor and W. Kanoknukulchai, 'A finite element method for large displacement contact and impact problems', in *Formulations and Computational Algorithms in Finite Element Analysis* (K. J. Bathe *et al.*, Eds.), M.I.T. Press, 1977.
7. L. R. Herrmann, 'Finite element analysis of contact problems', *J. Eng. Mech. Div.*, ASCE, **104** (EM5), 1043–1057 (1978).
8. N. Okamoto and M. Nakazawa, 'Finite element incremental contact analysis with various frictional conditions', *Int. j. numer. methods eng.*, **14**, 337–357 (1979).
9. J. L. Urzua and O. A. Pecknold, 'Analysis of frictional contact problems using an interface element', Proc. Symp. on Appl. of Computer Methods in Eng., Aug. 23–26, Los Angeles, CA, 1977.
10. L. T. Campos, J. T. Oden and N. Kikuchi, 'A numerical analysis of a class of contact problems with friction in elastostatics', *Comp. Meth. Appl. Mech. Eng.*, **34**, 821–845 (1982).
11. J. T. Oden and E. B. Pires, 'Nonlocal and nonlinear friction laws and variational principles for contact problems in elasticity', *J. Appl. Mech.*, ASME, **50**, 67–76 (1983).
12. J. J. Kalker, 'The computation of three-dimensional rolling contact with dry friction', *Int. j. numer. methods eng.*, **14**, 1293–1307 (1979).
13. J. J. Kalker, H. J. C. Allaert and J. de Mul, 'The numerical calculation of contact problem in the theory of elasticity', in *Nonlinear Finite Element Analysis in Structural Mechanics*, (W. Wunderlich *et al.*, Eds.), Springer-Verlag, 1981.
14. T. H. H. Pian and K. Kubomura, 'Formulation of contact problems by assumed stress hybrid elements', in *Nonlinear Finite Element Analysis in Structural Mechanics* (W. Wunderlich *et al.*, Eds.), Springer-Verlag, 1981.
15. C. S. Desai, M. M. Zaman, J. G. Lightner and H. J. Siriwardane, 'Thin element for interfaces and joints', *Int. J. Anal. Num. Meth. in Geomech.* (in press).
16. K. J. Bathe, *Finite Element Procedures in Engineering Analysis*, Prentice-Hall, 1982.
17. 'ADINA – A finite element program for automatic dynamic incremental nonlinear analysis', *Report AE 81-1*, ADINA Engineering, Watertown, MA 02172, and Vasteras, Sweden.
18. J. H. Dieterich, 'Time-dependent friction and the mechanics of stick–slip', *Pure Appl. Geophys.*, **116**, 790–806 (1978).
19. J.-C. Gu, J. R. Rice, A. L. Ruina and S. T. Tse, 'Slip motion and stability of a single degree of freedom elastic system with rate and state dependent friction', *Report Mech-41*, Div. of Applied Sciences, Harvard Univ. (March 1983).
20. E. Rabinowicz, *Friction and Wear of Materials*, Wiley, 1965.
21. S. P. Timoshenko and J. N. Goodier, *Theory of Elasticity*, McGraw-Hill, 1970, pp. 409–420.
22. G. Boman, Private communication.
23. M. Katona, 'A simple contact–friction interface element with applications to buried culverts', *Int. J. Num. Anal. Meth. Geomech.*, **7**, 371–384 (1983).